

Spatial linearity of unbalanced magnetic pull in induction motors during eccentric rotor motions

A. Tenhunen¹, T. P. Holopainen² and A. Arkkio¹

¹ Laboratory of Electromechanics

Department of Electrical and Communications Engineering, Helsinki University of Technology

P.O. Box 3000, FIN-02015 HUT, Finland

phone: +358 9 451 2382 – fax: +358 9 451 2991 - e-mail: Asmo.Tenhunen@hut.fi

² VTT Industrial Systems

Technical Research Centre of Finland

P.O. Box 1705, FIN-02044 VTT, Finland

e-mail: Timo.Holopainen@vtt.fi

Abstract — There is unbalanced magnetic pull between the rotor and stator of the cage induction motor when the rotor is not concentric with the stator. These forces depend on the position and motion of the center point of the rotor. In this paper, the linearity of the forces in proportion to the rotor eccentricity is studied numerically using time-stepping finite element analysis. The results show that usually the forces are linear in proportion to the rotor eccentricity. However, the closed rotor slots may break the spatial linearity at some operation conditions of the motor.

Introduction

An electrical motor converts electrical energy to mechanical work. The magnetic field in the air gap of the machine generates the tangential forces required for the energy conversion, but the field also produces other force components that may interact with machine structures and excite harmful vibrations. At low frequencies, the vibration amplitudes may be large enough to couple the electromagnetic system with the mechanical system. The electromechanical interaction changes the vibration characteristics of the machine e.g. it may induce additional damping or cause rotor dynamic instability.

The nature of these interaction forces has an effect on the methods required to model the electromechanical interaction in the machines. If the forces are linear in proportion to the rotor displacement, the electromagnetic and mechanical systems can be analysed separately and a highly reduced simulation model can be used to study the effects of electromechanical interaction.

Conventionally, the forces acting between the rotor and stator have been studied by analytical means. There is a lot of papers, in which the effects of the rotor eccentricity on the unbalanced magnetic pull are studied analytically (Freise and Jordan, 1962; Ellison and Yang, 1971; Smith and Dorrell, 1996; Belmans et al, 1987). The problem with the analytical models is how to evaluate the equalising currents induced in the windings by the asymmetric flux distribution. The effects of saturation and stator and rotor slotting are also difficult to model by analytical means.

Numerical field calculation methods have been used only rarely for calculating the forces due to eccentric rotors (Arkkio and Lindgren, 1992; Tenhunen, 2001). A time-stepping analysis is used for studying the effects of equalising currents induced by an eccentric rotor in the

parallel circuits of the stator windings on the forces (DeBortoli et al, 1993).

The references given above focus on the two special cases of whirling motion i.e. the static and dynamic eccentricity. However, the whirling motion of the rotor can also occur on some other frequencies. Früchtenicht et al. (1982) developed analytical tools to study the cage induction motor in a more general whirling motion.

Arkkio et al. (2000) presented a linear force model using complex variables for the electromagnetic forces acting between the rotor and stator:

$$\underline{F}(\omega_w) = \underline{K}(\omega_w)\underline{\varepsilon}(\omega_w) \quad (1)$$

in which \underline{F} is the total force, \underline{K} is the frequency response function of the system, $\underline{\varepsilon}$ is relative eccentricity, which is defined as a ratio between the whirling radius and average air-gap, and ω_w is the angular frequency of the whirling motion in relation to the stator. This model fits for non-synchronous whirling motion. They also determined the model parameters for an induction motor by numerical simulations and verified the results by measurements. Later on, this force model was incorporated with a mechanical rotor model and the interaction phenomena were studied (Holopainen et al, 2002). However, an important open question is the linearity of the forces in proportion to the eccentricity. The problem can be stated as: is it true that

$$\bar{F} = \bar{F}(\varepsilon, s, U, \omega_w) = \varepsilon \bar{F}'(s, U, \omega_w) \quad (2)$$

where s is the slip and U is the line voltage.

In this paper, the assumption of linearity is studied in order to establish the limits of application of this previously developed force model. The spatial linearity is studied numerically using impulse method (Tenhunen et al, 2002) in finite element analysis to calculate the frequency response functions between the forces and whirling radius of the rotor at different voltage and slip values. The results show that the assumption of the linearity is usually valid for small values of relative eccentricity. However, the closed rotor slots may break the linearity at some operation conditions.

Analytical study

At first, the analytical theory of the rotor eccentricity is presented briefly. The rotor eccentricity is considered as a

rotor in whirling motion. When the rotor is eccentrically positioned with respect to the stator bore, the air gap length δ is a function of the angular displacement x and time t

$$\delta(x, t) = \delta_0 [1 - \varepsilon \cos(x - \omega_w t - \varphi_w)] \quad (3)$$

where δ_0 is average air gap length and φ_w is the phase angle. The air gap permeance Λ varies inversely with the air gap length (Früchtenicht et al, 1982)

$$\Lambda(x, t) = \frac{\mu_0}{\delta(x, t)} = \sum_{\lambda=0}^{\infty} \Lambda_\lambda \cos[\lambda(x - \omega_w t - \varphi_w)] \quad (4)$$

with the Fourier coefficients

$$\Lambda_\lambda = \begin{cases} \frac{\mu_0}{\delta} \frac{1}{\sqrt{1-\varepsilon^2}} & \text{for } \lambda=0 \\ 2 \frac{\mu_0}{\delta} \frac{1}{\sqrt{1-\varepsilon^2}} \left(\frac{1-\sqrt{1-\varepsilon^2}}{\varepsilon} \right)^\lambda & \text{for } \lambda>0 \end{cases} \quad (5)$$

The magnetomotive force is assumed to be sinusoidally distributed in the air gap. The expression for the magnetomotive force is then

$$F_m(x, t) = \hat{F}_m \cos(px - \omega t - \varphi_m) \quad (6)$$

The magnetic flux density $b(x, t)$ is a product of magnetomotive force $F_m(x, t)$ and the air gap permeance $\Lambda(x, t)$

$$b(x, t) = F_m(x, t) \Lambda(x, t) \quad (7)$$

We consider only the motors, in which the number of pole pairs is bigger than one and neglect the homopolar flux by supposing that the integral of the flux density around the rotor is zero. Then, by taking only the first harmonics of the air gap permeance into account, the product in Equation (7) gives the flux density distribution in the air gap.

$$\begin{aligned} b(x, t) = & B_p \cos(px - \omega t - \varphi_m) + \\ & B_{p-1} \cos((p-1)x - (\omega - \omega_w)t - (\varphi_m - \varphi_w)) + \\ & B_{p+1} \cos((p+1)x - (\omega + \omega_w)t - (\varphi_m + \varphi_w)) \end{aligned} \quad (8)$$

where the amplitudes of the flux density harmonics are $B_p = F \Lambda_0$ and $B_{p\pm 1} = F \Lambda_{p\pm 1}$.

The radial component of the force between the rotor and stator to the z - and y -directions (vertical and horizontal directions with respect to the cross-sectional geometry) is got by surface integral over the rotor outer surface

$$\begin{aligned} F_z &= \int_0^{2\pi} \frac{b(x, t)^2}{2\mu_0} \cos(x) R l dx \\ F_y &= \int_0^{2\pi} \frac{b(x, t)^2}{2\mu_0} \sin(x) R l dx \end{aligned} \quad (9)$$

where l is the length and R is the outer radius of the rotor.

As a result, one gets the force vector, which rotates at the whirling frequency ω_w . The force vector is presented as complex form:

$$\underline{F} = \frac{\pi R l}{2\mu_0} (B_p B_{p-1} + B_p B_{p+1}) \cdot \{ \cos(x - \omega_w t - \varphi_w) + j \sin(x - \omega_w t - \varphi_w) \} \quad (10)$$

The force in Equation (10) presents only the radial component of the force. The forces are usually divided into the radial component in the direction of the shortest air gap and a tangential component perpendicular to the radial one. Früchtenicht et al. (1982) presented the common expression for the electromagnetic forces, including also the tangential component of the force.

The amplitude of the force vector depends only on the amplitudes of the permeance waves Λ , because the magnetomotive force \hat{F}_m is constant. Figure 1 shows the relative values of Fourier coefficients of the permeance waves Λ_0 and Λ_1 .

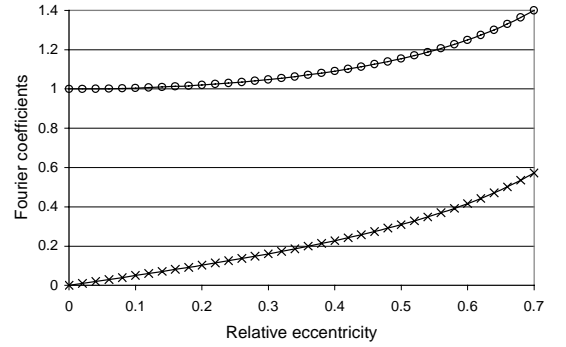


Figure 1. The Fourier coefficients of the permeance waves Λ_0 , marked by \circ , and Λ_1 , marked by \times as a function of relative eccentricity ε .

The radial component of the force is proportional to the product Λ of the Fourier coefficients of the permeance waves Λ_0 and Λ_1 . The product written as a series is

$$\Lambda = \left(\frac{\mu_0}{\delta} \right)^2 \left[\varepsilon + \frac{3}{4} \varepsilon^3 + \frac{7}{8} \varepsilon^5 + \frac{51}{64} \varepsilon^7 + \dots \right] \quad (11)$$

The first term in (11) is the linear part and the rest presents the non-linear part. Figure 2 shows the product and the relative error done when the forces are supposed to be linear in proportion to the displacement (sum of the non-linear terms in Equation (11)).

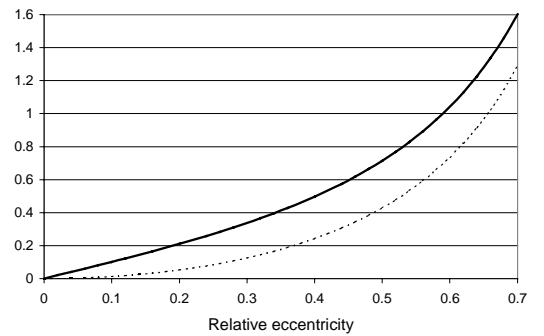


Figure 2. Product of the Fourier coefficients (thick line) and the error of the linear assumption (thin line).

Figure 2 shows that according to the analytical theory, the assumption of the spatial linearity is valid for small values of relative eccentricity.

This analytical study shows that the unbalanced magnetic pull is linear in proportion to the displacement of the rotor if the radius of the whirling motion, i.e. amplitude of the eccentricity is small. The effects of saturation are not taken into account in the analytical expression of the forces. The flux density harmonics created by the rotor eccentricity influence on the saturation and vice versa. That is why the spatial linearity is also studied numerically by time-stepping finite element analysis in the next section.

Method of numerical study

The calculation of the magnetic field and operating characteristics of the induction motor is based on time stepping finite-element analysis of the magnetic field. The details of the method are presented by Arkkio (1987). The magnetic field in the core region of the motor is assumed to be two-dimensional. End-winding impedances are used in circuit equations of the windings to model the end effects approximately. The magnetic field and circuit equations are discretized and solved together as a system of equations. The time-dependence of the variables is modelled by the Crank-Nicholson method. The method of analysis neglects the homopolar flux, but it should model properly the effects of equalising currents, slotting and saturation.

The method presented by Coulomb (1983) was used for computing the electromagnetic forces. It is based on the principle of the virtual work, and the forces are obtained as a volume integral computed in an air layer surrounding the rotor. In the two-dimensional formulation, the computation reduces to a surface integration over the finite elements in the air gap. The method was chosen because it has given accurate results when computing the forces of the electrical machines and it is verified by measurements (Arkkio et al, 2000). The forces are calculated at each time step and as a result one gets the forces as a function of simulation time.

The motion of the rotor is obtained by changing the finite-element mesh in the air gap. Second order, isoparametric, triangular elements were used. A typical finite-element mesh for the cross section of the test motors contained about 10000 nodes.

The impulse method in the finite element analysis is used to calculate the frequency response of the electromagnetic forces. The details of the impulse method are presented in reference (Tenhunen et al, 2002). The basic idea of the impulse method is to move the rotor from its central position for a short period of time to one direction, fixed into the stator co-ordinate system. This displacement excitation disturbs the flux density distribution in the air gap, and by doing this, produces forces between the rotor and stator. Using spectral analysis techniques the frequency response functions are determined using the excitation and response signals. The length T of the displacement pulse, which is defined $\varepsilon(t) = \varepsilon(1 - \cos(2\pi t/T))$, $t_1 < t < t_2$, was 0,01 s and the total simulation time was 1 s with constant time-step of 0.05 ms. To increase the spectral resolution, the sample size was extended to be 2 s obtained by adding the zeros to the end of the sample leading to frequency resolution of 0.5 Hz.

The discrete excitation and force signals were transformed into the frequency domain by the fast Fourier transform without filtering or windowing. The number of sample points was 8192.

The frequency response function presents the electromagnetic forces per whirling radius as a function of whirling frequency. Then, if the forces have spatial linearity property, the frequency response is independent of amplitude of the excitation pulse. The effective amplitude of the cosine excitation pulse is half of the maximum value.

Three parameters are varied in the analysis: the supply voltage, the amplitude of the displacement pulse, and the slip. The radial and tangential components of the frequency response of the electromagnetic forces are studied at range 0 – 50 Hz of whirling frequency, which is the fourth parameter in Equation (2). The limits of linearity are studied by varying the input parameters and comparing the frequency responses.

Results

Two machines, 15 kW and 37 kW four-pole cage induction motors were chosen for test motors to study the spatial linearity of the electromagnetic forces. The quarters of the cross-sectional geometry of the motors are shown in Figures 3 and 4 and the main parameters of the motors are presented in Table I. The main difference between these motors is that the 15 kW motor has open and the 37 kW motor closed rotor slots.

TABLE I. THE MAIN PARAMETERS OF THE TEST MOTORS.

Parameter	15 kW	37 kW
Number of poles	4	4
Number of phases	3	3
Number of parallel paths	1	1
Outer diameter of stator [mm]	235	310
Core length [mm]	195	249
Inner diameter of stator [mm]	145	200
Airgap length [mm]	0.45	0.8
Number of stator slots	36	48
Number of rotor slots	34	40
Connection	Delta	Star
Rated voltage [V]	380	400
Rated frequency [Hz]	50	50
Rated current [A]	28	69
Rated power [kW]	15	37



Figure 3. The cross sectional geometry of the 15 kW motor.

The values of the varied parameters in the analysis were the following: The used voltages were 100 V, 250 V and the rated voltage (380 V for 15 kW motor and 400 V for 37 kW motor). The used values for the slip were $s = 0\%$, $s = 1,6\%$ and $s = 3,2\%$ for 15 kW motor and $s = 0\%$, $s = 1,6\%$ for the 37 kW motor. The frequency response functions (FRF) were calculated using a displacement pulse with amplitudes 10 %, 20 % 30 % and 40 % of the air gap.

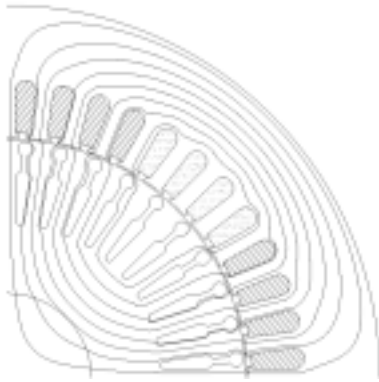


Figure 4. The cross sectional geometry of the 37 kW motor.

At first, the 15 kW motor, which has open rotor slots was studied. Figure 5 shows the FRF of the radial component and Figure 6 the FRF of the tangential component of the force. The voltages was 100 V and the slip $s = 0$ for all the used displacement pulses.

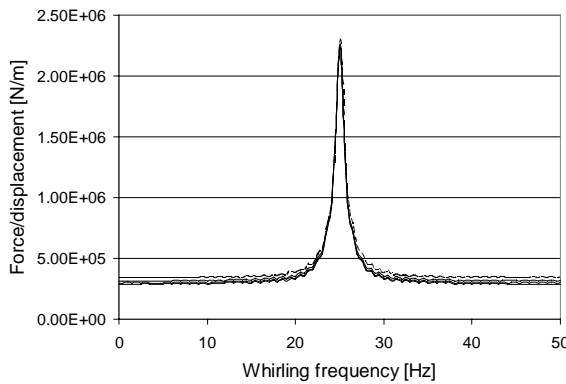


Figure 5. The radial components of the FRF function of the forces at $U=100\text{ V}$, $s=0\%$ for the 15 kW motor. The curves represent all the displacement pulses.

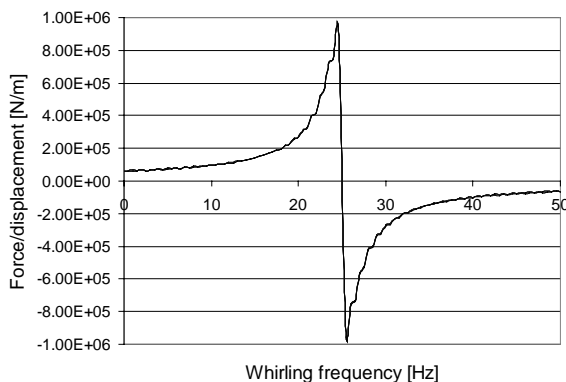


Figure 6. The tangential component of the FRF of the forces at $U=100\text{ V}$, $s=0\%$ for the 15 kW motor. The overlapping curves represent all the displacement pulses.

The radial component of the FRF grows slightly when the amplitude of the displacement pulse increases. In Figure 5, the upper most curve is calculated by a 40 % displacement pulse and the lowest is calculated by a 10 % pulse. The radial component of FRF by the 40 % displacement pulse is on average about 18 % larger than corresponding response calculated by the 10 % pulse. Anyway, the difference in the FRF is less than 10 % for the pulses of 20 % and 30 %.

The tangential component of the FRF seems to be independent of the amplitude of the pulse in this case. All the four responses in Figure 6 are almost equal, the maximum difference between them is less than 2 % of the amplitudes.

At voltage level 100 V, the maximum value of flux density is 0.69 T, so there are no saturation effects. At voltage 250 V, the maximum flux density is 1,32 T and the saturation slightly affects the magnetic field. Instead, at voltage 380 V, the motor is strongly saturated ($\hat{b} = 2.04\text{ T}$). Figure 7 and 8 present the FRF at rated operating point $U = 380\text{ V}$ and $s = 3,2\%$ for all the used displacement pulses.

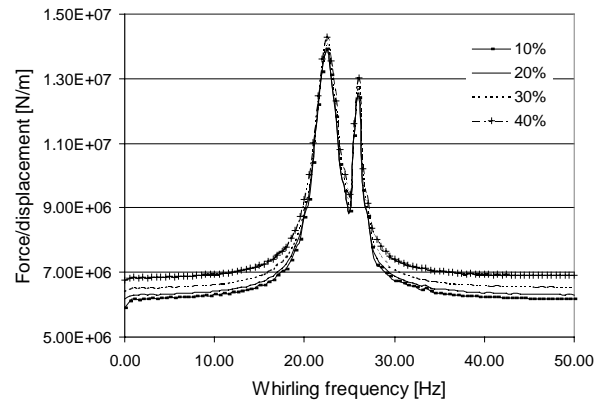


Figure 7. The radial components of the FRF of the forces at $U=380\text{ V}$, $s=3,2\%$ for the 15 kW motor.

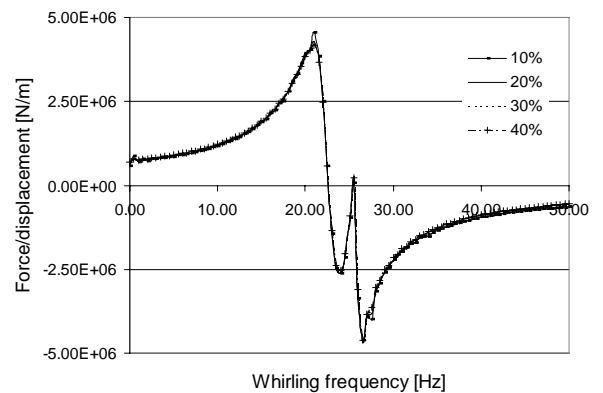


Figure 8. The tangential component of the FRF of the forces at $U=380\text{ V}$, $s=3,2\%$ for the 15 kW motor.

The frequency response functions presented in Figures 5-8 have a typical shape for the four pole cage induction motors. The behavior of the FRF as a function of the pulse amplitude is the same for all the calculated voltage levels. To study the spatial linearity more precisely, the electromagnetic forces are calculated from the FRF at whirling frequency 10 Hz. The behavior of the forces as a function of the displacement is similar at reduced voltage levels, so the results are presented only at voltage level 250

V. The radial and tangential component of the forces are presented as a function of the relative displacement in Figure 9 at 250 V and in Fig. 10 at 380 V voltage for slip values $s = 0\%$, $s = 1,6\%$ and $s = 3,2\%$.

According to the results presented in Figures 9 and 10, the tangential component of the force is almost linear function of the rotor displacement and it is independent of the slip. However, near to synchronous speed, the tangential component of the force depends strongly on the slip, but it still is a linear function of rotor displacement. The slip has a visible effect on the radial components of the forces. The radial component of the force follows the analytical theory well in the reduced voltages 100 V and 250 V.

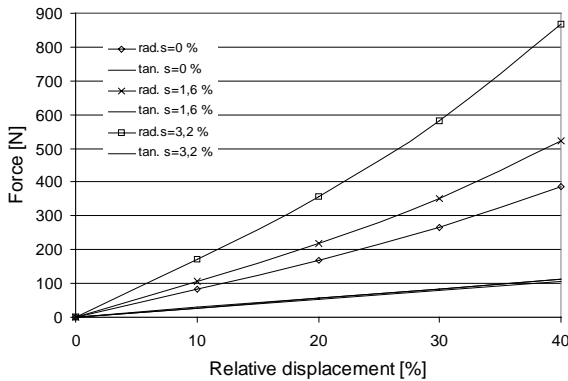


Figure 9. The forces as a function of relative displacement at 250 V and whirling frequency 10 Hz for the 15 kW motor.

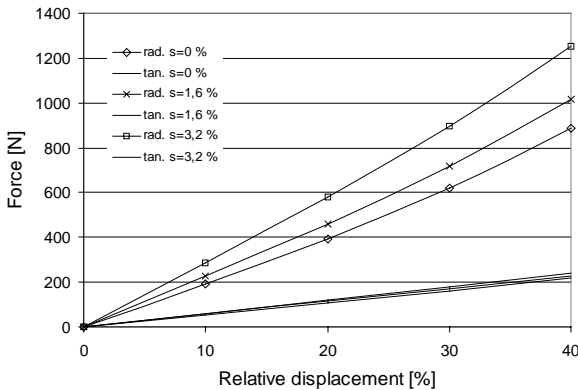


Figure 10. The forces as a function of relative displacement at 380 V and whirling frequency 10 Hz for 15 kW motor.

TABLE II. THE AVERAGE DIFFERENCE [%] OF THE TOTAL FORCE AS A FUNCTION OF DISPLACEMENT PULSE COMPARED WITH THE TOTAL FORCE CALCULATED BY 10% DISPLACEMENT PULSE FOR THE 15 kW MOTOR. THE TOTAL FORCES ARE CALCULATED VARYING VALUES OF VOLTAGE AND SLIP.

U=100 V	s = 0 %	s = 1,6 %	s = 3,2 %
20%	2.2	3.1	4.8
30%	6.4	9.2	14.5
40%	14.4	20.7	33.7
U=250 V			
20%	2.2	3.0	4.0
30%	6.3	9.0	11.5
40%	14.3	19.9	24.3
U=380 V			
20%	2.0	2.0	1.7
30%	5.9	5.5	4.7
40%	12.5	11.0	9.1

Table II presents the average difference of absolute value of the total force at whirling frequency range 0 – 50 Hz as a function of displacement pulse compared with the total force calculated by 10% displacement pulse. The difference is calculated by calculating the difference of the absolute value for each of the studied whirling frequencies and taking the average of the differences at valid frequency range. The total forces are calculated varying the values of voltage and slip.

According to Table II, the frequency response of the forces is almost the same for 10% and 20% rotor displacements. We can assume that the spatial linearity is valid for smaller than 10% displacements.

Actually, Table II shows the error, which results when using the assumption of spatial linearity, at different values of relative rotor displacement for different operating characteristic of the motor.

After the analysis of the 15 kW motor, the spatial linearity is studied for the 37 kW motor. Figure 11 presents the FRF of the radial component and Figure 12 the FRF of the tangential component of the force at voltage 400 V in no load condition ($s = 0\%$) for all the used displacement pulses.

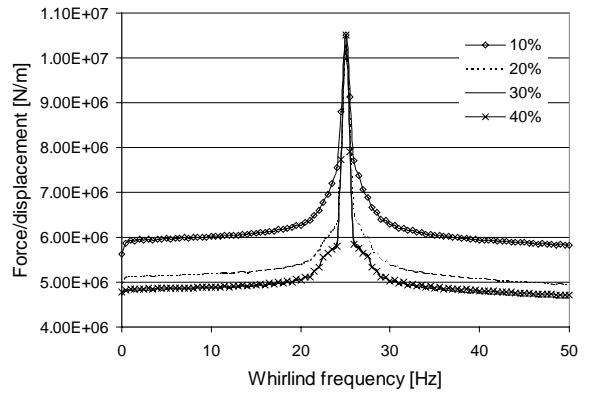


Figure 11. The radial components of the FRF of the forces at U=400 V, s=0% for the 37 kW motor.

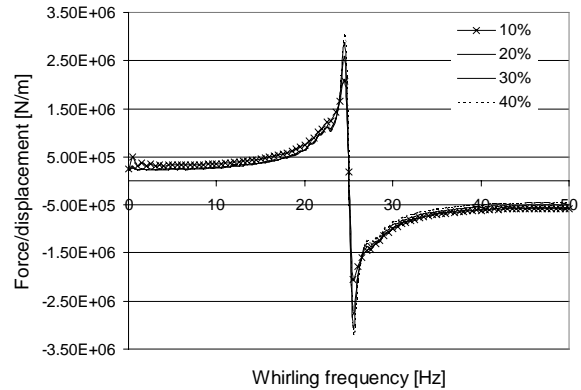


Figure 12. The tangential component of the FRF of the forces at U=400 V, s=0% for the 37 kW motor.

Figure 11 shows the nonlinear behavior of the forces at this operating point and used displacements. The smallest pulse gives the largest radial component of the FRF. The exception is the synchronous speed, at which no equalizing currents are induced into the rotor cage and the FRF is independent on the pulse. The closed rotor slots can explain the nonlinear behavior. The eccentricity harmonics in Equation (8) open magnetically the rotor slots and the damping currents start to flow in the rotor cage when the

amplitude of the displacement increases. The tangential components of the FRF (Figure 12) are almost equal for all the pulses. However, at whirling frequencies near to the synchronous speed the 10 % pulse gave notably lower forces.

Table III presents the average difference of absolute value of the total force at whirling frequency range 0 – 50 Hz as a function of displacement pulse compared with the total force calculated by 10 % displacement pulse for 37 kW motor. The total forces are again calculated varying values of voltage and slip.

The same effect, which is shown in Figure 11, seems to occur also at all the studied voltage levels at no load. If the rotor displacements increase, the saturation level in the iron over the rotor slots increases, and more and more induced damping currents flow in the rotor cage. The induced currents in rotor cage damp the harmonics created by the rotor displacement, and by doing this, damp nonlinearly the forces and break the spatial linearity property at relatively low values of rotor displacement.

TABLE III. THE AVERAGE DIFFERENCE OF THE TOTAL FORCE [%] AS A FUNCTION OF DISPLACEMENT PULSE COMPARED WITH THE TOTAL FORCE CALCULATED BY 10 % DISPLACEMENT PULSE FOR THE 37 kW MOTOR. THE TOTAL FORCES ARE CALCULATED VARYING VALUES OF VOLTAGE AND SLIP.

U=100 V	s = 0 %	s = 1,6 %
20%	-16.0	5.4
30%	-23.2	17.6
40%	-24.2	47.0
U=250 V		
20%	-7.5	4.3
30%	-10.7	13.5
40%	-7.7	31.8
U=400 V		
20%	-13.7	3.1
30%	-19.1	8.0
40%	-18.7	15.9

At rated load, the force – rotor displacement relation follows approximately the analytical expression. The absolute value of the total force increases slightly when the rotor displacements increase.

Discussions

The 15 kW cage induction motor has open rotor slots. The saturation has hardly no effects on the forces. The increase of the load linearises slightly the forces in proportion to displacement. For the 37 kW test motor, the saturation effects are more complicated. At no load condition, the harmonics created by rotor displacement open magnetically the rotor slots through the saturation when the displacement grows enough. For loaded motors, the fundamental field opens the slots and the spatial linearity is valid.

However, the amplitudes of the vibrations are usually very small, just few percents of the air gap. Based on this fact, obtained results indicate that the assumption of the spatial linearity is valid for studying the electromechanical interaction. One should be aware of the possibility that the

closed rotor slots may cause nonlinearity at some operating points of the motor.

Conclusions

The linearity of the electromagnetic forces between the rotor and the stator in proportion to the rotor displacement is studied in this paper. At first, the background of the study is presented analytically. The spatial linearity is studied numerically using time-stepping finite element analysis. The results indicate that usually the forces are linear in proportion to the rotor displacement. However, the closed rotor slots may break the spatial linearity of the forces at some operating points of the motor.

References

- Arkkio, A. (1987), Analysis of induction motors based on the numerical solution of the magnetic field and circuit equations, Acta Polytechnica Scandinavica Electrical Engineering Series, No. 59, Helsinki.
- Arkkio, A. and Lindgren, O. (1994) "Unbalanced magnetic pull in a high-speed induction motor with an eccentric rotor", Proceedings of IECM'94, September 5-8, 1994, Paris, France, pp. 53-58.
- Arkkio, A., Antila, M., Pokki, K., Simon, A. and Lantto, E. (2000) "Electromagnetic force on a whirling cage rotor", IEE Proceedings – Electric Power Applications, Vol. 147, No. 2, pp. 353-360.
- Belmans, R., Vandenput, A. and Geysen, W. (1987) "Calculation of the flux density and the unbalanced pull in two pole induction machines", Archiv für Elektrotechnik, Vol. 70, pp. 151-161.
- Coulomb, J. L. (1983) "A methodology for the determination of global electro-mechanical quantities from a finite element analysis and its application to the evaluation of magnetic forces, torques, and stiffness", IEEE Transactions on Magnetics, Vol. 19, No. 6, pp. 2514-2519.
- DeBortoli, M. J., Salon, S. J., Burow, D. W. and Slavik, C. J. (1993) "Effects of rotor eccentricity and parallel windings on induction machine behavior: a study using finite element analysis", IEEE Transactions on Magnetics, Vol. 29, No. 2, pp. 1676-1682.
- Ellison, A. J. and Yang, S. J. (1971) "Effects of rotor eccentricity on acoustic noise from induction machines", Proceedings of IEE, Vol. 118, No. 1, pp. 174-184.
- Freise, W. and Jordan, H. (1962) "Einseitige magnetische Zugkräfte in Drehstrommaschinen", ETZ-A, (Germany), Vol. 83, No. 9, pp. 299-303.
- Früchtenicht, J., Jordan, H. and Seinsch, H. O. (1982) "Exzentrizitätsfelder als Ursache von Laufinstabilitäten bei Asynchronmaschinen, Parts 1 and 2", Archiv für Electrotechnik (Germany), Vol. 65, pp. 271-292.
- Holopainen, T. P., Tenhunen, A. and Arkkio, A. (2002) "Electromagnetic circulatory forces and rotordynamic instability in electric machines", in Proceedings of 6th International Conference on Rotor Dynamics, 30.9 - 3.10.2002. Sydney, Australia, pp. 456-463.
- Smith, A. C. and Dorrell, D. G. (1996) "Calculation and measurement of unbalanced magnetic pull in cage induction motors with eccentric rotors. Part 1: Analytical model", IEE Proceedings - Electric Power Applications, Vol. 143, No. 3, pp. 193-201.
- Tenhunen, A. (2001) "Finite-element calculation of unbalanced magnetic pull and circulating current between parallel windings in induction motor with non-uniform eccentric rotor", Proceedings of Electromotion'01, June, 19-20, 2001, Bologna, Italy, pp. 19-24.
- Tenhunen, A., Holopainen, T. P. and Arkkio, A. (2002) "Impulse method to calculate the frequency response of the electromagnetic forces on whirling cage rotors", Proceedings of CEFC'2002, June 16-19, 2002, Perugia, Italy, p. 109.